Kinetic modelling of parallel ion transport in the SOL and divertor of inter-ELM JET high radiative H-mode plasma

A.V.Chankin[1] , G.Corrigan[2], A.E.Jaervinen[3] and JET Contributors*

EUROfusion Consortium, JET, Culham Science Centre, Abingdon, OX14 3DB, United Kingdom
[1]Max Planck Institut für Plasmaphysik, Garching bei München, Boltzmannstr. 2, 85748, Germany
[2]CCFE, Culham Science Centre, Abingdon, OX13 3DB, United Kingdom
[3]Lawrence Livermore National Laboratory, Livermore, California 94550, United States of America

Abstract

KInetic code for Plasma Periphery (KIPP) was used to assess the importance of kinetic effects of parallel ion transport in the scrape-off layer (SOL) and divertor of JET high radiative H-mode inter-ELM plasma conditions with strong nitrogen (N_2) injection, leading to partial detachment at divertor targets. Plasma parameter profiles along the magnetic field from one of the EDGE2D-EIRENE simulation cases were used as an input for KIPP runs. The profiles were maintained by particle and power sources. This work is a continuation of the previous study carried out for electrons [1].

In this modelling KIPP calculated ion distribution functions and ion parallel power fluxes. In the main SOL kinetic effects lead to a reduction of heat (conductive power) fluxes compared to Braginskii fluxes by factors 3 to 4 ('heat flux limiting'). In the divertor, on the contrary, a strong 'heat flux enhancement', by up to two orders of magnitude above Braginskii's, was found. Similar to cases for electrons, high ion heat flux enhancement factors, in particular near targets, are attributed to a non-local transport of super-thermal ions originating from positions along field lines with the highest ion temperature, resulting in the appearance of bump-on-tail features on ion heat flux density profiles. Despite ion heat flux enhancement factors at the target being much higher than for electrons, total power fluxes, ion plus electron, were dominated by ion and electron convection and electron conduction, with ion conductive fluxes playing a secondary role. This must be attributed to lower ion (than electron) velocities (factor $\sim\sqrt{m_e/m_i}$ reduction), which aren't compensated by kinetic effects of lower ion upstream collisionality.

*See the author list of "Overview of the JET preparation for Deuterium-Tritium Operation", by Joffrin E. *et al* 2019 Nucl. Fusion **59**, 112021

1. Introduction

KIPP is a continuum Vlasov-Fokker-Planck code for parallel plasma transport in the scrape-off layer (SOL) and divertor. Main equations, including normalization of parameters, are described in [2]. The code combines an implicit 2^{nd} order scheme for a full non-linear Coulomb collision operator with an explicit 2^{nd} order scheme for the free-streaming, see [2] for details. Results of the code benchmarking can be found in [3] and refs. therein.

The code was recently upgraded to include kinetic treatment of an arbitrary number of ion species. It was also extended to enable radial (across magnetic surfaces) exchange of distribution functions, making it a 2D2V code, with 2 spatial variables (along magnetic field lines and across flux surfaces) and 2 velocity variables: parallel and gyro-averaged perpendicular velocities. Ion species designated as 'impurities' don't necessarily have to be modelled kinetically, instead they can serve as Coulomb centres for 'ion' species, which are to be modelled kinetically. This effect is achieved by summing up impurities' Rosenbluth potentials, assuming drifting Maxwellian distribution functions for each impurity species, and adding them to those calculated for ions.

The present work is an extension of the earlier modelling with kinetic electrons [1], where KIPP cases were run using parallel (along magnetic field lines) profiles of plasma parameters calculated by EDGE2D-EIRENE code, which in turn simulated an inter-ELM JET high radiative H-mode plasma with 8 MW of input power and 5 MW of radiated power on nitrogen impurities, with the input power into the computational grid split equally between ion and electron channels. In KIPP runs, macroscopic parameters (density, temperature, parallel velocity) were maintained by particle and power sources, yielding kinetic parallel plasma transport coefficients. In this work similar runs were carried out for ions in the presence of impurities.

Apart from supplying information about the behaviour of super-thermal charged particles on their way from high temperature upstream SOL down to the divertor and, finally, to divertor target plates, such a modelling represents an important step towards the final goal of the KIPP development: its iterative coupling to the 2D edge fluid code SOLPS. An algorithm of a coupling scheme, where SOLPS provided macroscopic plasma parameter profiles to KIPP, with KIPP returning kinetic transport coefficients to SOLPS, was successfully tested in [4]. Only ~ 5 iterative steps were sufficient to reach a steady state coupled KIPP-SOLPS solution [4]. Such a solution satisfies all conservation laws enforced by SOLPS, contains realistic magnetic geometry in the SOL and divertor, as well as Monte-Carlo calculations of neutrals and their interaction with the plasma using EIRENE, and at the same time satisfies the Vlasov-Fokker-Planck equation for ion and electron distribution functions stored in spatial cells.

Despite KIPP presently having a facility to exchange distribution functions between neighboring cells in the radial direction (being technically a 2D2V code, see above), the work on derivation of coefficients for mixing f-functions at each time step compatible with EDGE2D (or SOLPS) diffusive fluxes has not yet been done. According to present priorities of the KIPP development this should be done after the implementation of the KIPP-SOLPS coupling. Hence, the modelling described here is not using the potential 2D feature of the code, and KIPP runs are carried out only along selected filed lines, in the 1D2V mode.

It has to be pointed out that inelastic ion-neutral processes in KIPP are not treated kinetically. They are part of the preceding EDGE2D-EIRENE run, with EIRENE assuming Maxwellian ion distribution functions. One of the presently discussed options to assess the importance of kinetic effects, primarily of charge exchange collisions between ions and neutrals, is to approximately match the kinetic ion distribution function with two Maxwellians having different densities, temperatures and parallel velocities, and then specify them as two different fluids in EIRENE runs.

In this paper the setup of KIPP cases is described in Section 2. Ion and electron collisionalities in the selected EDGE2D-EIRENE case are calculated in Section 3. KIPP results for flux tubes at different radial positions in the SOL ('slices') are presented in Section 4. Section 5 is dedicated to analysis of the structure of ion power fluxes to the target, giving examples of bump-on-tail features of power flux density profiles vs. absolute velocity. Results of this work are summarized in Section 6.

2. Setup of KIPP cases

Details of the setup of the EDGE2D-EIRENE case can be found in [1]. For running KIPP cases, the basic approach, based on the output from EDGE2D-EIRENE, was explained in the previous section. The cases were run separately for each radial position, analogously with runs described in [1] for electrons, along magnetic field lines in the SOL and divertor, from one target to the other, with parallel distances counted from the inner target, IT, to the outer target, OT, for 6 radial positions indicated by vertical arrows in Fig. 1. This figure also shows radial profiles of ion and electron temperatures $T_{i,e}$ and electron density n_e at the outer midplane position (OMP). As in [1], flux tubes along which KIPP calculations were carried out will be referred to as 'slices', with slice numbers 'i' shown above vertical arrows in Fig. 1.

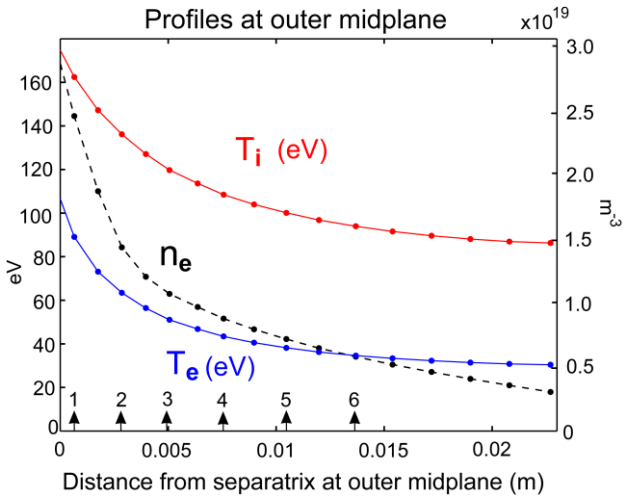

Figure 1. Radial profiles of ion and electron temperatures and electron density at the outer midplane (OMP) position.

Fig. 2, replicated from [1], gives the expanded view of the EDGE2D grid in the divertor region, with positions of slices 1 to 6 indicated. Arrows indicate the direction of counting the parallel distance, from the inner to outer target, projected onto poloidal plane.

The only species to be modelled kinetically were deuterium (main working gas) ions D^+, since they carry most of the heat flux. 11 impurity species: 4 for beryllium (Be) and 7 for nitrogen (N), were not modelled kinetically. For them, instead, drifting Maxwellian distributions with densities and parallel velocities taken from the EDGE2D-EIRENE solution were assumed, and Coulomb collisions between ions (D^+) and 'impurities' (11 species) were calculated as explained in the previous section. Since in EDGE2D temperatures of all impurity species are equal to the temperature of main ions, no ion-impurity energy equipartition power sources occured in KIPP runs.

It may be questioned whether specifying Maxwellians for impurities' distribution functions can be applied to e.g. Be ions due to their small charge, but modelling Be ions kinetically wouldn't make any significant impact on KIPP solutions for D^+ due to very low Be ion concentrations in the EDGE2D-EIRENE solution. The most populous impurity species were N^{+4} and N^{+5} which have short collision mean free paths (MFP) and therefore low heat fluxes. Since, unlike in the case of electron kinetic modelling, D^+ (referred to as 'ions' below) Coulomb collisions with impurities can't be described by any single parameter such as Z_{eff}, Rosenbluth potentials of all 11 impurity species, as well as those for ions (D^+) must be summed up. Transport coefficients in the velocity space for ion collisions with ions and impurities are then calculated based on the Rosenbluth potentials and their derivatives, as described e.g. in [2].

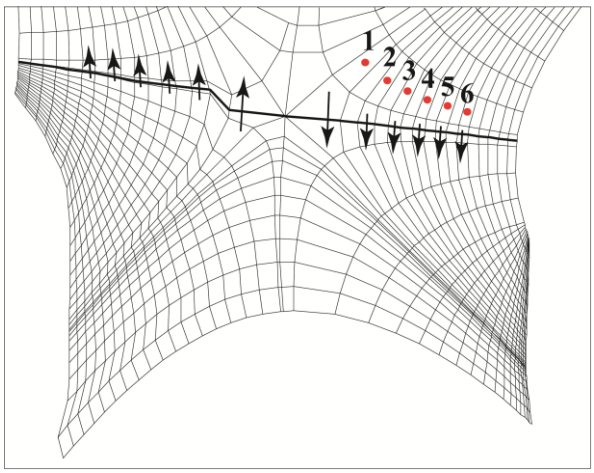

Fig. 2. Expanded view of the EDGE2D grid in the divertor region, showing numbered cells corresponding to radial positions of poloidal 'rings' (using EDGE2D nomenclature) which were chosen for KIPP runs. The chosen rings are referred to as 'slices' (for KIPP runs). Their numbering, given by index 'i' in the paper, doesn't coincide with the ring numbering in EDGE2D. Replicated from [1].

In KIPP runs for ions, normalizations are done analogously to runs for electrons. Instead of the maximum T_e along the field line (or the flux tube), the maximum T_i, $T_{i,max}$, which is always in the same spatial cell as that with the maximum T_e, is used for the normalization of energy for all cells along the field line (in the 'parallel' direction), separately for each slice. Electron density in the cell with $T_{i,max}$ is taken for normalization of all ion and impurity densities. Ion thermal velocity $\sqrt{T_{i,max}/m_i}$, with m_i being D^+ mass, is used for normalizations of parallel velocities. The normalization of time is done by using $T_{i,max}$ and n_e in the same cell, according to the Braginskii formula for electron collision time [5], but with ion, instead of electron, temperature and mass. Finally, parallel distance is normalized by using the product of the ion collision time and ion thermal velocity, as a unit of distance.

In most physical processes involving ions and electrons, except for the e-i equipartition energy exchange, collisions between ions and electrons (i-e collisions) can be neglected compared to ion-ion (i-i) collisions. Therefore in dimensionless variables equations to be solved in KIPP for calculating ion kinetic power fluxes are exactly the same as equations for electrons where only electron-electron (e-e) Coulomb collisions are taken into account, ignoring electron-ion (e-i) collisions. In a dedicated test case with a strongly collisional pure D^+ plasma, with 10% T_i drop from one target to the other, ion parallel conductive power flux in the middle of the spatial grid following from the KIPP run matched Braginskii ion parallel heat flux (Eq. (2.15) of [5]) within 0.5% accuracy.

In this paper the 'conductive power flux' will often be referred to as 'heat flux'. KIPP results for this quantity and their comparison to Braginskii's formula will be of prime interest. As for the convective (ion) power flux, it can be calculated by using T_i, V_i (ion average parallel velocity) and n_i (ion density) profiles along field lines which in KIPP runs were maintained to

match those following from the EDGE2D-EIRENE solutions, as pointed out in the previous section.

As for electron kinetic calculations [1], the same dimensionless logarithmic velocity grid with the 2% increase in the linear grid size from cell to cell, beginning from the origin (zero parallel and perpendicular velocities), with 400×200 velocity cells (400 for parallel velocity, which may be both positive and negative, and 200 cells for perpendicular gyro-averaged velocity), and with boundary velocities equal to $v_i/\sqrt{T_{i,max}/m_i} = 7$, with m_i being D^+ mass, was used for ions for all slices. For large T_i variations along field lines from upstream to divertor targets it allows for a satisfactory velocity grid resolution for ion distribution functions f_i in spatial cells with highest and lowest T_i.

Similarly to KIPP runs for electrons [1], the number of grid cells in the poloidal direction of the EDGE2D grid was increased by factor 2, from 88 to 176, by dividing each cell in half and interpolating EDGE2D-EIRENE output profiles from original to new, thinner cells, which were used for KIPP runs. As explained in [1], with KIPP being a 2nd order code relying on linear interpolations between cell centre and cell face values, such an increase in spatial cell numbers results in smoother output profiles by reducing cell to cell variations in input (EDGE2D-EIRENE) profiles.

As in [1], toroidal effects were accounted for in KIPP calculations described here, see Sec. 6 of this Ref. for details of their implementation in KIPP. In difference to electrons, where toroidal effects were hardly visible in the code output, in ion kinetic calculations they made a significant impact on KIPP solutions, increasing parallel power fluxes by factors ~ 1/3. While electron parallel and perpendicular temperatures, $T_{e\|}$ and $T_{e\perp}$, respectively, were very close to each other, within 2%, $T_{i\|}$ and $T_{i\perp}$ can be quite different, by factor ~ 2.

3. Upstream collisionality of ions and electrons in the SOL

Owing to their relatively low ion and electron temperatures, scrape-off layer (SOL) and divertor plasmas in tokamaks are usually considered to be collisional, with charged particles being in the strong collisionality Pfirsch-Schlüter regime, in which 'fluid' plasma transport equations, formulated e.g. in [5], can be applied. In one important respect, however, namely in the application to parallel heat transport, plasma collisionality is often insufficient to justify the use of such equations. It is well known that even in the strongly collisional SOL the bulk of parallel heat flux is carried by much less collisional high energy super-thermal charged particles with kinetic energies in the range of 5 to $9T_e$ for electrons, according to [6,7]. By assuming that parallel velocities of heat carrying electrons (HCE) is ~ $3v_{th}$, with $v_{th} = \sqrt{T_e/m_e}$, and using the $(v/v_{th})^4$ scaling for the MFP of super-thermal electrons for Coulomb collisions, the factor of ≈ 80 increase in this quantity for MFP of HCE compared to thermal electrons was predicted in [8]. This would have made HCE almost fully collisionless for typical SOL conditions. Dedicated analysis of contributions of electrons with different parallel and perpendicular energies to the parallel power flux density $f_e m_e v^2 v_{\|}/2$, with $v_{\|}$ and v being parallel and total electron velocities, however revealed that the factor 80 must be a gross overestimate. By using $v_{\|}$ and v at which the quantity $f_e m_e v^2 v_{\|}/2$ peaks, and taking into account the effect of e-e in addition to e-i collisions, it was shown that dimensionless electron collisionality is only by factor ~ 13 lower than for thermal electrons, defined as

$\nu_e^* = L_\parallel/(\tau_{e,coll} v_{e,th})$, where $\tau_{e,coll}$ is electron collision time calculated according to Eq. (2.5e) for τ_e in [5], $v_{e,th}$ is electron thermal velocity and $L_\parallel$ - parallel connection length [1]. Correspondingly, HCE turn out to be substantially more collisional than it could be concluded by using simple scalings, with the consequence that electron heat flux following from kinetic calculations must also diverge from Braginskii values to a much lesser extent than expected [1].

In the upstream SOL ions are much less collisional than electrons for two reasons. Firstly, only self i-i collisions are important for ions, compared to both e-i and e-e collisions for electrons. This gives approximately factor 2 increase for the ion MFP compared to electron. Secondly, and more importantly, T_i is typically by factor ~ 2 higher than T_e in the SOL, see e.g. T_e and T_i profiles from an output of the EDGE2D-EIRENE case in Fig. 1.

Experimental measurements confirm that the ratio T_i/T_e in the SOL is almost always above unity, unless the plasma density is low and a specific method of heating electrons is used. According to experimental results collected from different tokamaks in the review paper [9], in the conduction limited regime in the SOL T_i is systematically higher than T_e. In particular, at the separatrix position, among large and medium-sized machines, the T_i/T_e ratio was found to be ≈ 2 in JET, TEXTOR and Tore Supra, and ≈ 3.5 in JT-60U [9]. Since collisionality scales with ion temperature as T_i^{-2}, it gives another factor ~ 4 reduction in ν_i^* compared to ν_e^*. One should therefore expect much stronger kinetic effects, in particular a much stronger influence of non-local ion kinetic effects on the ion heat flux than in the case of electrons.

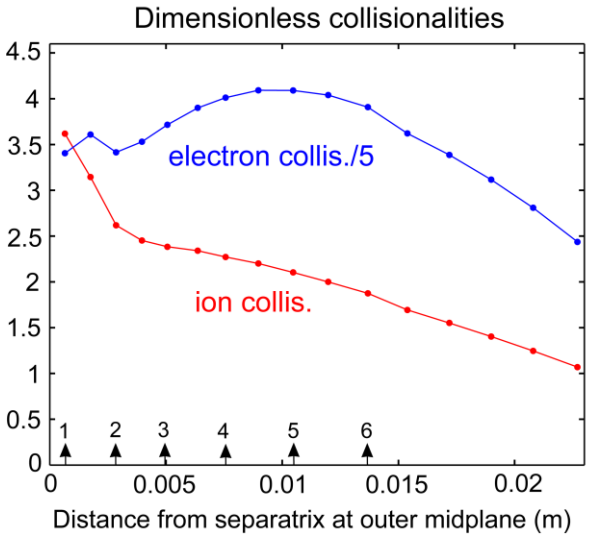

Figure 3. Dimensionless ion and electron collisionalities calculated for cells with the highest $T_{e,i}$ along field lines, calculated according to Eqs. (1,2).

For OMP profiles shown in Fig. 1, focusing on the influence of kinetic effects of charged particle transport towards more important (receiving higher power flux) outer target (OT), we calculate dimensionless collisionalities by taking the connection length $L_\parallel$ to be equal to the parallel distance between the cell with the highest $T_{e,i}$ and that adjacent to OT. For electrons, using the above formula for ν_e^*, we will use:

$$\nu_e^* = \frac{L_\parallel}{\tau_{e,coll} v_{e,th}} \approx 10^{-16} L_\parallel(\mathrm{m}) \frac{n_e(\mathrm{m}^{-3})}{T_e(\mathrm{eV})^2}. \qquad (1)$$

This formula coincides with Eq. (4.105) in [10], which uses the same definition of $\tau_{e,coll}$ as in [5].

For D^+ ions we use a slightly different formula, which approximately reflects longer

collisional MFP for ions than electrons, by choosing Eq. (2.5i) for τ_i in [5], rather than using the same expression as for τ_e with only replacing electron with ion parameters. Note that in [5] the numerical coefficient for τ_i is larger than for τ_e by factor $\sqrt{2}$, hence:

$$\nu_i^* = \frac{L_\parallel}{\tau_{i,coll} v_{i,th}} \approx 10^{-16}\sqrt{2} \times L_\parallel(m) \frac{n_e(m^{-3})}{T_i(eV)^2}. \qquad (2)$$

Both formulas are rather approximate by ignoring the presence of impurities, therefore n_e rather than n_i is used in Eq. (2).

Dimensionless collisionalities calculated by using Eqs. (1,2) and OMP profiles from Fig. 1, are shown in Fig. 3. At slice 1, closest to the separatrix, ion collisionality is by factor ~ 5 lower than electron. For more outward slices, owing to a steeper T_e than T_i drop across the SOL (in Fig. 1 the T_i/T_e ratio increases from 1.69 at zero distance from the separatrix to 2.82 at the end of the grid) the ratio ν_e^*/ν_i^* is even higher. Ion dimensionless collisionalities not significantly exceeding unity imply that ions upstream are in a weakly collisional regime.

4. KIPP results for slices i = 1 and 6, and power fluxes at outer target for all slices

Similarly to the previous paper [1] for kinetic electrons, we will only present detailed results for slices i = 1 and 6. In slice 1, upstream $T_{e,i}$ are the highest, while the divertor is in a high recycling regime with partial detachment at the targets, with target $T_{e,i}$ below 1 eV. In slice 6 the drop in $T_{e,i}$ from the upstream to the targets is quite moderate, and the divertor is also in a moderate recycling regime. Parameters in slices 2 to 5 are transitional between the two extremes, i = 1 and 6. Some results, e.g. power fluxes at OT, will be presented for all slices.

We shall start with slice i = 1. Parallel profiles from the inner to outer target of T_i, T_e, n_e, Z_{eff} and parallel ion (D^+) velocity $V_{i\parallel}$ are shown in Fig. 4. These are all output results of the EDGE2D-EIRENE run. Vertical dashed lines indicate positions of entranced to (inner and outer) divertors. Maximum T_i and T_e are 164.1 and 90.4 eV, respectively, while T_i at inner and outer targets are 0.27 and 0.78 eV, respectively, with T_e values being very close to T_i due to high plasma collisionalities near targets. Target profiles of T_e, n_e and ion saturation current density j_{sat} can be found in Fig. 5 of [1]. Z_{eff} in the 'main SOL' (the part of the SOL excluding the divertor) is ~ 2, implying average nitrogen impurity density ~ 3×10^{18} m^{-3} (the main impurity species are N^{+4} and N^{+5}). Near divertor targets $Z_{eff} \approx 1$, as impurities are being

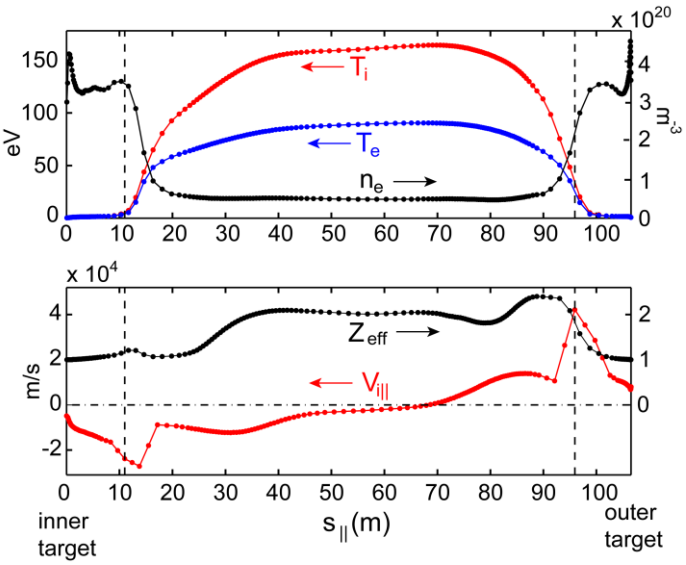

Figure 4. Parallel profiles of ion and electron temperatures, electron density, Z_{eff} and parallel ion velocity for slice i = 1, vs. distance along field lines. Vertical dashed lines indicate positions of entrances to the divertor.

pushed out of the divertor into the main SOL by the ion-impurity thermoforce caused by the T_i drop towards the targets.

Results of KIPP runs for parallel power fluxes are shown in Fig. 5. In most of the main SOL ion conductive power flux ('heat flux') from KIPP, $q_i^{cond,KIPP}$, is lower than that from EDGE2D-EIRENE, $q_i^{cond,EDGE2D}$, by factors 3 to 4, indicating heat flux limiting due to super-thermal ions escaping from the upstream plasma because of their low collisionality, which is a well known effect of the non-local kinetic transport (see. e.g. review paper [11]). For electrons this ratio is ~ 1.5 [1], indicating that ion kinetic effects are stronger than electron, as expected based on ions' lower collisionality (see previous section). Steep rises in ion convective power flux q_i^{conv} towards divertor entrances is caused by plasma acceleration manifested by the $V_{i\|}$ rise in Fig. 4. In the EDGE2D-EIRENE modelling such a steep q_i^{conv} rise is balanced by a similarly steep drop in $q_i^{cond,EDGE2D}$. Contrary to this, in KIPP calculations near the entrance to the outer divertor, due to 'heat flux enhancement' downstream [11], $q_i^{cond,KIPP}$ doesn't show such a sharp drop as $q_i^{cond,EDGE2D}$. An apparent rise in the total, conductive plus convective, ion KIPP flux through the entrance to the outer divertor is a consequence of the setup of KIPP cases in which power source is used to maintain the parallel T_i profile following from EDGE2D-EIRENE. This suggests that a very sharp T_i fall across the entrance to the outer divertor, with T_i falling by factor > 2 between the two neighboring cells from each side of the entrance (second vertical dashed line in Fig. 4), is an artifact of using a fluid code in EDGE2D: if strong non-local ion kinetic effects were taken into account, such a steep T_i drop would have not been possible.

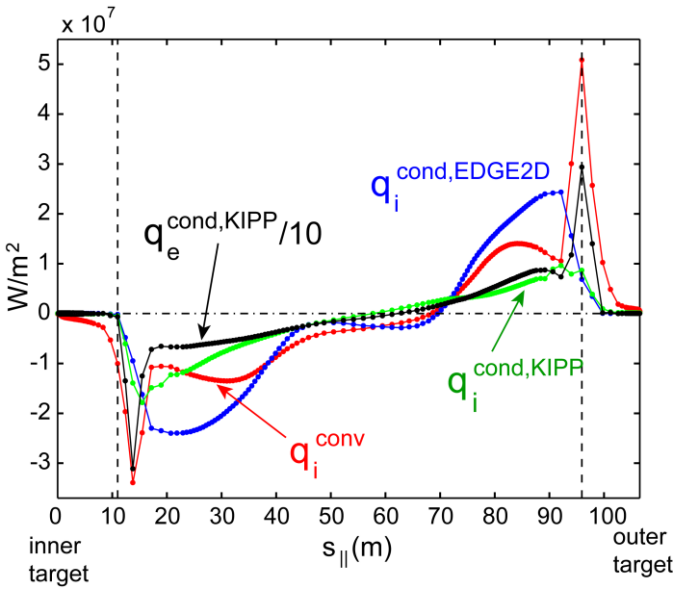

Figure 5. Parallel profiles of ion conductive power flux from EDGE2D-EIRENE and KIPP, ion convective power flux, and electron conductive power flux divided by 10, for slice i = 1, vs. distance along the field line. Vertical dashed lines indicate positions of entrances to the divertor.

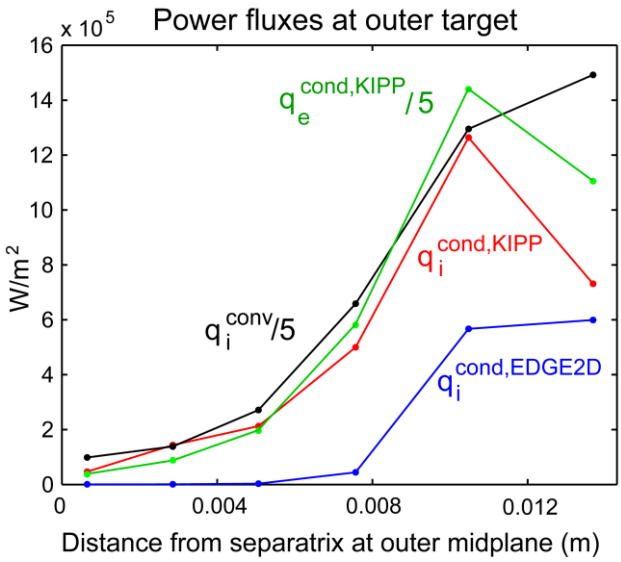

Figure 6. Power fluxes at the outer target for all slices i vs. distance from the separatrix increasing from i = 1 to i = 6.

In addition to ion power fluxes, electron heat flux $q_e^{cond,KIPP}$ divided by 10 is also plotted in Fig. 5. This heat flux is substantially higher than any of ion power fluxes, which can be attributed to a much smaller mass of electrons than ions: for example, in the strong collisionality limit, as follows from equations for electron (Eq. (2.12)) and ion (Eq. (2.15)) heat fluxes in [5], for $T_e = T_i$ electron heat flux is by factor $\sqrt{m_i/m_e}/1.745$ (≈ 34 for D^+) larger than ion. Owing to $T_i > T_e$, however, as follows from the same equations, the difference between the two heat fluxes must be less than factor 34.

Power fluxes in the divertor and at targets can't be resolved in Fig. 5. Instead, we shall here plot power fluxes at OT for all slices in Fig. 6. Related to the slice i = 1 discussed above are power fluxes at the leftmost position in this figure. The smallest power flux is $q_i^{cond,EDGE2D} \propto \kappa_i \nabla T_i$, where coefficient $\kappa_i \propto T_i^{5/2}$ [5] and ∇T_i is the T_i gradient along parallel distance. Owing to smallness of T_i this power flux is negligible. The heat flux $q_i^{cond,KIPP}$ is by factor $\approx$ 70 higher than $q_i^{cond,EDGE2D}$ due to the contribution of strongly non-local heat flux from super-thermal ions discussed in the next section. However, high density, low temperature plasma in the divertor strongly attenuates this heat flux, making it factor ≈ 10 lower than the convective flux q_i^{conv}. This means that ion power flux is carried to the OT mostly by convection. Electron heat flux is much higher than ion, but lower than q_i^{conv} by factor ≈ 1.9. Since, owing to almost equal T_e and T_i at the target, ion and electron convective power fluxes are close to each other, we conclude that the total, ion plus electron, power flux to OT at this slice is carried mostly by convection. It has to be noted that among all 6 slices power fluxes for slice i =1 are the lowest due to partial detachment conditions with high density and very low temperatures at the target.

We now proceed to slice i = 6. Moderate $T_{i,e}$ drops from upstream to targets are related to a moderate neutral recycling level in the divertor, leading to a moderate n_e variation in the divertor, see Fig. 7. In the EDGE2D-EIRENE solution for this slice, which belongs to the 'outer SOL', negative ion velocity $V_{i||}$ covering the whole main SOL in the direction from the outer to inner divertor can be seen.

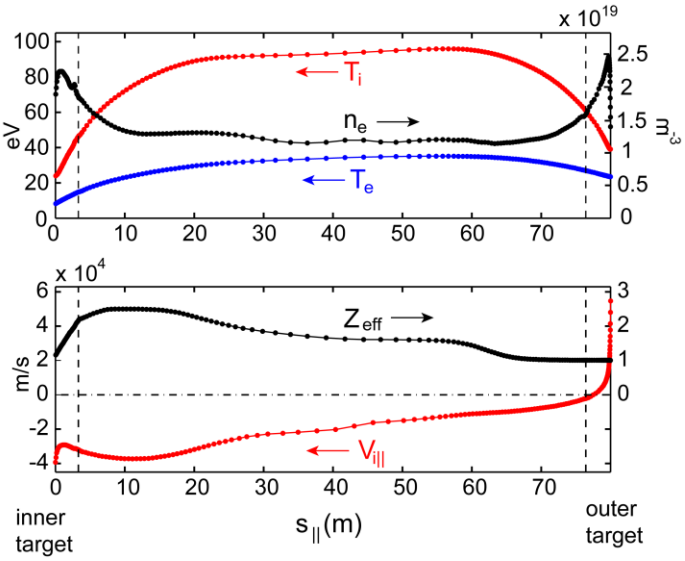

Figure 7. The same parallel profiles as shown in Fig. 4, but for slice i = 6. Vertical dashed lines indicate positions of entrances to the divertor.

The negative parallel ion particle flux in the main SOL causes a large ion convective power flux from the outer to inner divertor, as can be seen in Fig. 8, which shows the same profiles as in Fig. 5, but for slice i = 6. A significant difference, up to factor ~ 5, between $q_i^{cond,EDGE2D}$ and $q_i^{cond,KIPP}$ in favour of the former, can be seen in the figure. This difference is larger than for slice i = 1, which must be related to lower ion collisionality for this slice than for i = 1, as follows from Fig. 3, resulting in stronger heat flux limiting upstream. At OT, $q_i^{cond,KIPP}$ is not very different from $q_i^{cond,EDGE2D}$, as can be seen in Fig. 6. A significant deviation of $q_i^{cond,KIPP}$ from $q_i^{cond,EDGE2D}$ couldn't be expected since the T_i drop from the highest value upstream, $T_{i,max}$, to OT is only a factor ≈ 2.5.

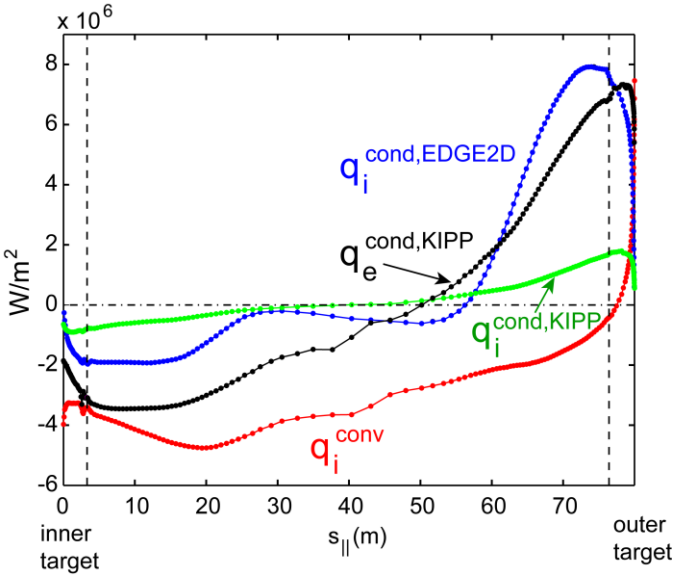

Figure 8. The same parallel profiles as shown in Fig. 5, but for slice i = 6. Vertical dashed lines indicate positions of entrances to the divertor.

Ion convective power flux q_i^{conv} at OT is significantly higher than both $q_i^{cond,EDGE2D}$ and $q_i^{cond,KIPP}$, as can be seen in Fig. 6, making ion convection the main mechanism to carry ion energy to the target. This should be attributed to a smaller role of ion heat conduction in the total ion power flux due to factor $\sim\sqrt{m_e/m_i}$ of the reduction of the ion heat flux compared to electron, as was pointed out above.

As can be seen in Fig. 8, $q_e^{cond,KIPP}$ is substantially higher than $q_i^{cond,KIPP}$, as it is also the case for slice i =1 (Fig. 5). The same relation holds also for power fluxes at OT (Fig. 6), and not only for slices 1 and 6, but for all other slices as well. This again must be the consequence of the factor $\sim\sqrt{m_e/m_i}$ reduction of ion compared to electron heat fluxes. At the same time, q_i^{conv} and $q_e^{cond,KIPP}$ at OT are not too far off from each other for all slices (Fig. 6). We can therefore conclude that dominant power flux mechanisms in both the main SOL and divertor regions are electron heat conduction and convection (both ion and electron, which are not very different). At the same time ion heat conduction plays a secondary role in parallel energy transport in the SOL and divertor, despite ions being much less collisional than electrons in the main SOL.

5. Bump-on-tail features on ion heat flux density profiles in the divertor

Under conditions of very high density and low temperatures in the divertor, with strong reduction of power fluxes to the target, covering slices 1 to 4, $q_i^{cond,KIPP} >> q_i^{cond,EDGE2D}$ at both targets (but results only for OT are presented here). It is of interest to analyse the structure of ion kinetic heat fluxes at the target. For this analysis we will use power flux

density $\langle f_i v_\parallel v^2/2 \rangle$, where $v_\parallel$ and v are parallel and absolute ion velocity in the ion rest frame, moving with the averaged parallel ion velocity. Here the averaging is done for a given absolute velocity v, vs. normalized total ion velocity v/v_{th}, with $v_{th} = \sqrt{T_{i,max}/m_i}$ and $T_{i,max}$ being the highest ion temperature along a field line (a slice). Such a representation of the heat flux density has a benefit of highlighting contributions of super-thermal ions due to the presence of the velocity space factor (the surface of a sphere, $\propto v^2$, over which the averaging $\langle ... \rangle$ is done). It can be found e.g. in Fig. 7 of Ref. [7] for electrons. A qualitatively similar profile can be seen in Fig. 9d for slice i = 6 in this paper.

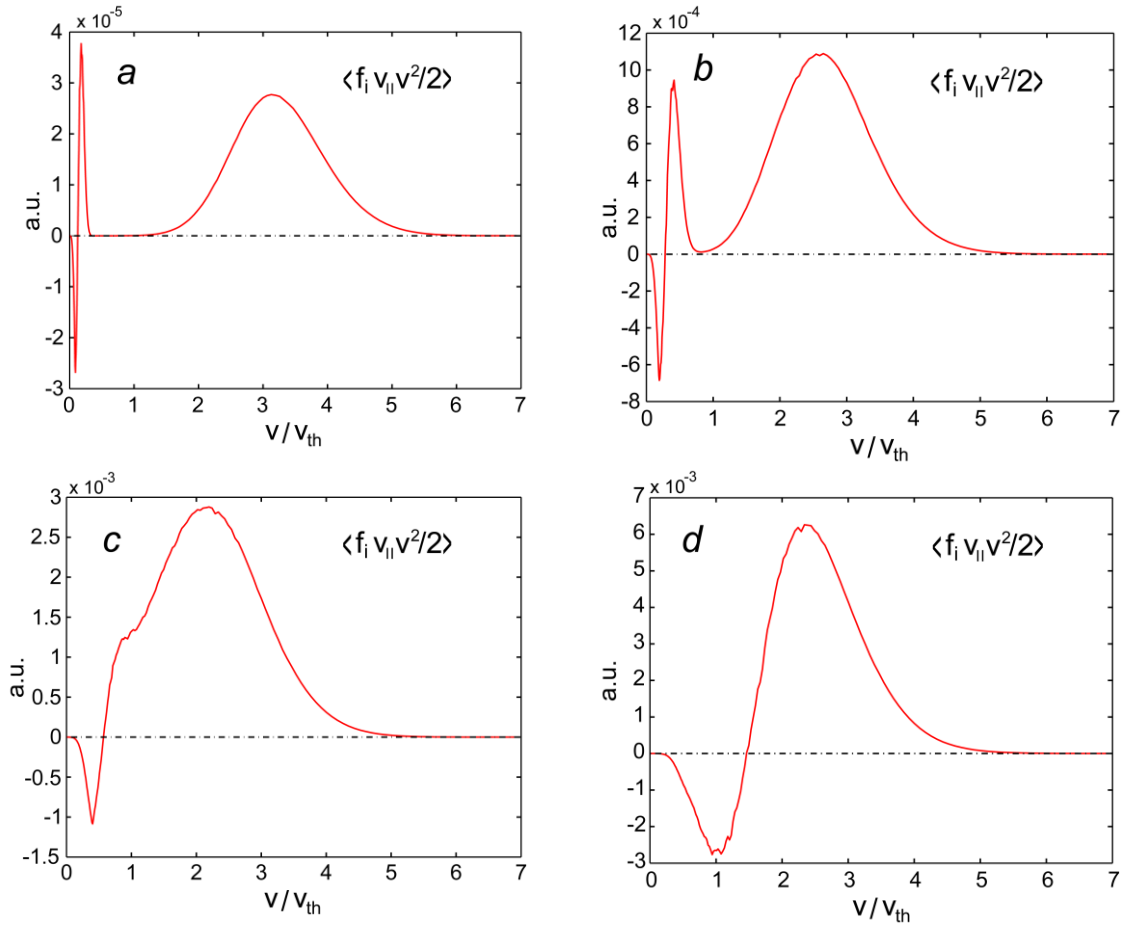

Figures 9a-d. Ion heat flux densities vs. dimensionless total velocity, using f_i at cells adjacent to the outer target for slices i = 1 (a), 4 (b), 5 (c) and 6 (d).

Figures 9a-d show heat flux density profiles for slices 1,4,5 and 6, respectively. The choice of slices presented reflects qualitative changes in profiles which will be explained below. The normalized total ion velocity v/v_{th} uses the highest ion temperature along the field line for each slice, $v_{th} = \sqrt{T_{i,max}/m_i}$, as stated above. If, instead, the local T_i was used, the maximum of the second, positive oscillation for the slice i = 1 (Fig. 9a) at $v/v_{th} \approx 0.2$ would have been at $v/v_{th} \times \sqrt{T_{i,max}/T_{i,OT}} \approx 0.2 \times \sqrt{164.1/0.78} \approx 2.9$, which is much closer to its location in dedicated KIPP tests for the ion heat flux in strongly collisional plasma (≈ 3.5). The reason for heat fluxes being negative at low v/v_{th} (first, negative oscillation in Fig. 9a)

is the subtraction of the average parallel velocity in the heat flux density calculations for both $v_\parallel$ and v^2 quantities in $\langle f_i v_\parallel v^2/2 \rangle$, so that this average is calculated in the reference frame of a drifting f_i with $\bar{v}_\parallel = 0$, where more energetic ions have predominantly positive $v_\parallel$, while less energetic – negative $v_\parallel$.

The two oscillations at low v/v_{th} in Fig. 9a therefore reflect the contribution from the part of f_i which is close to a Maxwellian (to be referred to as 'Maxwellian core' below), reflecting very high collisionality for most of ions near OT. On top of it one can see an extended bump-on-tail feature. Judging by the velocity of its maximum, at $v/v_{th} \approx 3$, it should be attributed to the heat flux of super-thermal ions coming from far upstream, from the zone of highest ion temperatures along the field line. Their transport towards the divertor is strongly non-local, but due to Coulomb collisions being concentrated mostly in the dense (high density) divertor, power flux carried by these ions is strongly attenuated, with most of super-thermal ions being thermalised, resulting in a rather low total power flux at OT compared to that for other slices, especially those in the outer SOL, i = 5 and 6 (see Fig. 6). At the same time, even this small flux by almost two orders of magnitude exceeds the heat flux calculated according to the Braginskii formula for strongly collisional plasma, which is very close to $q_i^{cond,EDGE2D}$. It has to be pointed out that the above mentioned zone of highest ion temperatures along the field line is rather wide, for example, the zone of $T_i > 150$ eV in Fig. 4 covers ≈ 55% of the whole parallel length of the main SOL, between the two vertical dashed lines. It is therefore capable of generating a fairly high non-local power flux. Similar bump-on-tail features were also seen for electron heat fluxes [1], but for electrons, due to their much higher collisionality compared to ions, such features have much lower amplitudes.

Ion heat flux density profiles for slices i = 2 and 3 are similar to that for slice i = 1. They show a gradual increase in velocities corresponding to the oscillations as well as a gradual decrease in velocities of the maximum of bump-on-tail features (which will be interpreted below), until the oscillations begin to merge with the wide bump-on-tail feature, as shown in Fig. 9b for i = 4. For this slice the divertor is still in a very high recycling regime, $T_{i,OT} = 2.5$ eV, resulting in a very low $q_i^{cond,EDGE2D}$ at OT, as can be seen in Fig. 6. The second (positive) spike of the Maxwellian core is at $v/v_{th} \approx 0.4$, reflecting both an increase in $T_{i,OT}$ and a decrease in $T_{i,max}$ (111.4 eV).

The ion heat flux density profile for slice i = 5 (Fig. 9c) shows an almost complete overlap between the second (positive) spike and the bump-on-tail feature. $T_{i,OT} = 8.5$ eV for this slice, resulting in a sharp increase in $q_i^{cond,EDGE2D}$. Finally, the ion flux density profile for slice i = 6 (Fig. 9d) loses the bump-on-tail feature completely, making it look qualitatively similar to that for a KIPP test case for a strongly collisional plasma. For this slice, with the divertor being is a moderate recycling regime, $T_{i,OT} = 39$ eV, $T_{i,max} = 96$ eV.

We would next like to give a possible explanation for the origin of bump-on-tail features on ion heat flux density profiles in regimes with very high recycling, high plasma density in the divertor and a large $T_{i,max}/T_{OT}$ drop. It may be reasoned, at the first glance, that, since T_i monotonically falls from the cell with the highest temperature, $T_{i,max}$, to the lowest T_i at the target, the heat flux density profile at OT should also be a monotonically falling function of

v/v_{th} (here we are leaving aside oscillations at low v/v_{th} discussed above). This is because super-thermal ions 'emitted' from different positions along the field line should all contribute to the heat flux at the target, with those emitted from far upstream having a larger probability to reach the target due to their higher energies (hence fewer collisions with bulk ions), while those emitted from e.g. entrance to the divertor having a larger probability to reach the target because of the shorter distance to the target. This would have partly equilized probabilities of reaching the target for ions emitted from different locations. Such a reasoning however can't be applied, because most of i-i collisions take place in the divertor, where plasma density by far exceeds that in upstream regions, and ions emitted from any location in the SOL all have to undergo collisions with approximately the same number of background ions. Therefore super-thermal ions emitted from the entrance to the divertor have no advantage in their probability to reach the target, while those emitted from upstream locations with the highest T_i do have such an advantage owing to their lower collisionalities. Since the collision MFP for super-thermal ions scales as v^4, ions emitted from the region with T_i close to $T_{i,max}$ must have the largest probability of reaching the target without being thermalised. This explains why the peak value of the part of the ion heat flux density belonging to the bump-on-tail feature is approximately at $v/v_{th} = 3$. This ratio follows from the analysis of the maximum of the heat flux density, being a compromise between factors favouring high v/v_{th} (higher energy, lower collisionality, higher volume in velocity phase space) and the exponential factor of falling numbers of such ions $\propto \exp(-v^2/2v_{th}^2)$.

An opposite situation exists for conditions with a moderate recycling in the divertor and a moderate $T_{i,max}/T_{OT}$ ratio, not greatly exceeding unity. In such conditions energies of super-thermal ions emitted from different places along the field line are not too much different from each other, and the T_i profile along the field line is much flatter, hence contributions of super-thermal ions emitted from different places along the field line to the heat flux at the target to a much greater extent represent a superposition of individual contributions from all locations. This explains why, as the ratio $T_{i,max}/T_{OT}$ starts to fall, the peak heat flux of the bump-on-tail feature gets shifted to lower v/v_{th}, until, at relatively low $T_{i,max}/T_{OT}$ ratio ~ 1, the bump-on-tail feature gets completely blended into the second (positive) oscillation of the heat flux density profile. This creates a standard profile of the ion heat flux density existing in strongly collisional plasma, with $v/v_{th} \approx 3$ at the location of the second (positive) oscillation.

Despite super-thermal ions originating from the upstream zone with T_i close to $T_{i,max}$ not being able to carry enough power to the target to influence the total power flux onto it, they might be important for the target erosion. For $T_i \approx 150$ eV, the energy of super-thermal ions from the bump-on-tail feature is ~ $7 \times T_i \approx 1$ keV. As was shown in laboratory tests [12], deuterium bombardment of the tungsten (W) surface, which is exposed to the plasma fluxes in the divertor of JET, as well as in the ITER experimental fusion reactor, sputters ~ 5×10^{-2} W atoms per D atom (or ion) with the incident energy of 1 keV [12]. The sputtering yield curve is very steep, and for D energies below 200-300 eV there is almost no sputtered W, hence the Maxwellian core of the dense and cold plasma near the divertor target makes zero contribution to the target sputtering. The particle flux associated with energetic ions from the bump-on-tail feature is however quite low, by factor ≈ 13000 lower than the flux attributable to bulk ions at the target with $T_i \approx 1$ eV.

The D sputtering however is unlikely to be the dominant contributor to the total target

sputtering. For the same energy of an incident W impurity ion of 1 keV the W self-sputtering yield is ≈ 1 (see Fig. 8 in [13]). It is unlikely that such high energy W ions can reach the target in the near SOL region with detachment, owing to very low T_i near the target and large equipartition energy exchange between W and D ions. At the same time, in the outer SOL, with $T_e \approx 30$ eV at the outer target (see Fig. 5 of [1]), a W^{10+} ion diffusing out of the hot core plasma, can gain energy ~ $Z_i \times 3 \times T_e \approx 1$ keV by accelerating in the Debye sheath and magnetic pre-sheath at the target (see calculations in [13]), sputtering on average one W atom. Possible tungsten divertor erosion in ITER based on JET experiments with ITER-like wall was analysed in [14]. The role of Be sputtering, as well as seeded impurities sputtering (N, Ne), especially during ELMs, was found to be more important than D sputtering.

6. Summary

KIPP modelling shows that in the SOL of the JET high radiative H-mode inter-ELM plasma ion kinetic effects are much stronger than electron owing to lower ion collisionality. In the upstream SOL longer ion mean free paths (MFP) are caused primarily by a substantially higher ion temperature, with the T_i/T_e ratio varying approximately between factors 2 to 3 across the SOL. Another reason for the longer ion MFP is that only i-i collisions are important for ions, whereas for electrons – both e-e and e-i collisions are important.

Upstream in the near SOL (close to the separatrix) due to kinetic effects of the heat flux limiting, ion heat flux is by factors 3 to 4 lower than that calculated using Braginkii heat flux formula (for electrons this factor is ~ 1.5 [1]). Downstream in the divertor, under conditions of a partial detachment from the target, a very high heat flux enhancement is predicted by KIPP, with the target ion heat flux being by two orders of magnitude higher than the Braginskii heat flux (for electrons – only one order of magnitude higher [1]). As in the case for electrons, most of the ion heat flux is carried by a strongly non-local parallel transport of super-thermal ions originating from upstream SOL regions with the highest T_i along the field line. Heat flux density profiles reveal bump-on-tail features responsible for the bulk of the target heat flux. Owing to ions' lower upstream collisionalities, bump-on-tail features are more pronounced for ions than for electrons.

Despite kinetic effects of ion parallel transport being much stronger than for electrons due to their lower collisionality, they are playing only a secondary role in the plasma energy transport towards the divertor target. The main contributions to the total power flux, both upstream and at the target, come from electron power conduction and ion plus electron power convection, at least for conditions analysed here. Ion convective power fluxes to the target are much higher than conductive power fluxes ('heat fluxes') due to very low T_i at the target, making Braginkii heat fluxes almost negligible, so that even with high heat flux enhancement factors ion heat fluxes to the target are still much below ion convective power fluxes. The main reason for kinetic effects of ion parallel transport not being able to significantly alter total (ion plus electron) parallel power fluxes, both in the near and far SOL, as well as both upstream in the SOL and in the divertor, is their low parallel velocities, by factor $\sqrt{m_e/m_i}$ (1/60 for deuterium ions) lower than for electrons (for the same temperatures), and this factor can't be compensated by kinetic effects related to lower ion than electron collisionality in the upstream SOL. It could be that the most significant impact of ion kinetics in the SOL on macroscopic plasma parameters is an increase in the upstream T_i due to the heat flux limiting. The degree of such an increase will be assessed in future coupled KIPP-SOLPS cases.

Acknowledgement

This work has been carried out within the framework of the EUROfusion Consortium and has received funding from the Euratom research and training programme 2014-2018 and 2019-2020 under grant agreement No 633053. The views and opinions expressed herein do not necessarily reflect those of the European Commission. Discussions with Dr. D.P.Coster and a significant contribution of Dr. H.Leggate as part of the High Level Support Team (HLST) in 2017 and 2019 in structuring KIPP, extending it from 1D to 2D, and incorporating tools for inclusion of an arbitrary number of ion species, are acknowledged.

References

[1] Chankin A V, Corrigan G, Jaervinen A E, and JET Contributors 2018 Plasma Phys. Control. Fusion **60** 115011
[2] Chankin A V, Coster D P, and Meisl G 2012 Contrib. Plasma Phys. **52** 500
[3] Chankin A V and Coster D P 2015 J. Nucl. Mater. **463** 498
[4] Zhao M, Chankin A V, Coster D P 2019 Comput. Phys. Commun. **235** 133
[5] Braginskii S I 1965 'Transport processes in a plasma', *Review of Plasma Physics* Vol. 1, edited by M.A.Leontovich (Consultants Bureau, New York) p.205
[6] Gray D R and Kilkenny J D 1980 Plasma Phys. **22** 81
[7] Chodura R 1988 Contrib. Plasma Phys. **28** 303
[8] Kupfer K *et al* 1996 Phys. Plasmas **3** 3544
[9] Kočan M *et al* 2011 J. Nucl. Mater. **415** S1133
[10] Stangeby P C 2000, The Boundary of Magnetic Fusion Devices, IOP Publishing, Bristol
[11] Fundamenski W 2015 Plasma Phys. Control. Fusion **47** R163
[12] Sugiyama K, Schmid K, Jacob W 2016 Nucl. Mater. and Energy **8** 1
[13] Chankin A V, Coster D P, Dux R 2014 Plasma Phys. Control. Fusion **56** 025003
[14] van Rooij G J *et al* 2013 J. Nucl. Mater. **438** S42